Interactive Medical Image Segmentation using Active Contour with Improved *F* Energy in Level-Set Tuning

Khosro Rezaee[1*], Mohammad Khalil Nakhl Ahmadi[2], Maryam Saberi Anari[3*]
1- Department of Biomedical Engineering, Meybod University, Meybod, Iran.
Email: kh. rezaee@meybod.ac.ir (Corresponding author)
2- Islamic Azad University, Torbat-e Jam Branch, Torbat-e Jam, Iran.
Email: khalilahmadi752@gmail.com
3- Department of Computer Engineering, Technical and Vocational University (TVU), Tehran, Iran.
Email: saberi-m@tvu.ac.ir

Received: October 2021 Revised: December 2021 Accepted: Februarty 2022

ABSTRACT:
Segmentation is a fundamental element in Medical Image Processing (MIP) and has been extensively researched and developed to aid in clinical interpretation and utilization. This article discusses a method for segmenting abnormal masses or tumors in medical images that is both robust and effective. We suggested a method based on Active Contour (AC) and modified Level-set techniques to detect malignancies in Magnetic Resonance Imaging (MRI), mammography, and Computed Tomography (CT). To segment malignant masses, the active contour approach, the energy function, the level-set method, and the proposed F function are employed. The system was evaluated using 160 medical images from two databases, including 80 mammograms and 80 MRI brain scans. The algorithm for segmenting suspicious segments has an accuracy, recall, and precision of 96.25%, 95.60%, and 95.71%, respectively. By adding this technique into tissue imaging devices, the accuracy of diagnosing images with a relatively large volume that are evaluated fast is increased. Cost savings, time savings, and high precision are all advantages of the approach that set it apart from similar systems.

KEYWORDS: Image Processing, Medical Image, Highboost, Active Contour, Levelset, F-Energy.

1. INTRODUCTION

Medical images are a proper tool for examining tissue abnormalities [1]. Because of technological breakthroughs, people are living longer and having a better quality of life. Surgical planning using functional simulation [2,3], morphological techniques [4], and medical image analysis increases the pressure on medical operators, who are also demanded to undertake increasingly tailored and patient-specific operations. Therefore, even when target anatomical structures can be seen using an imaging modality like CT, MRI, ultrasound, and other medical imaging methods, the bottleneck is typically automatically identifying and delineating (segmentation) of them [5]. Patient-specific processes are still uncommon in most healthcare applications due to a dearth of manual annotations. There are a number of issues with medical images: they're complex in structure and detail, and have poor contrast [6]. There are different ways to segment the section of medical images so that each of them can accomplish by various techniques [7]. Over the last few decades, different algorithms have been performed for image segmentation, from region growing [8], thresholding [9.10], and clustering [11] to active contour patterns (ACPs) [12-15]. Deep Learning (DL) has remarkably developed the performance of several segmentation processes, principally benefitting from their substantial capacity to learn hierarchical features straight from images [16]. However, they require a large number of images and take a lot of time in training [17].

Popular techniques such as thresholding, edge detection, and region of interest (RoI) segmentation are employed in various image processing analyses [18]. However, these approaches do not play a constructive role due to the loss of the original image data, changes in main contents, and low accuracy in segmentation process. The contour method (level curves) is considered an image classification technique that uses the set of variable parameters and geometric properties to classify the image regions [19]. The early contour idea was introduced by Osher and Sethian, during which the original contour curves were formed from the edge structures and influence of certain conditions of the image [20-22]. Internal states of the curve led to more smooth and diffraction in the image. One of active contours modeling is parametric techniques in which the

Paper type: Research paper
DOI: https:// 10.30486/mjee.2022.696492
How to cite this paper: Kh. Rezaee, M. Khalil Nakhl Ahmadi and M. Saberi Anari,"**Interactive Medical Image Segmentation using Active Contour with Improved F Energy in Level-Set Tuning**", Majlesi Journal of Electrical Engineering, Vol. 16, No. 2, pp. 21-30, 2022.

main parameter of the loop iteration takes new values in the contour expansion process. Despite the high-speed process, setting the parameters by the user is difficult.

In contrast, the level-set method (i. e., setting the contour line) is a quite intelligent strategy for segmentation and separation of multiple parts of the image. A level-set model begins in 2D space with an initial curve to grow and, accordingly, achieves stability based on the defined target in the image. The level-set calculation method uses mathematics and contrasts geometric parameter procedure, which is not met with any stipulations. Thus, the contour line method is considered as a proper segmentation tool for tracing specific objects in images not to alter the input original image data. Unlike parametric models that use explicit equations [23], active contours are geometric models whose spatial coordinates are the functional model from parameters in the image.

Weickert and et al. [24] proposed fast active contours in complex models to detect interesting segments of the image. Holtzman and Goldshe [25] presented ranking segmentation of the images based on the active contours model. Rosher and et al. [26] (2004) introduced the Graph Cuts method for segmenting the image. In 2006, Foo [27] developed active contours in a medical image texture to segment-specific regions. Boykov, in the same year, used the model Graph Cuts and its impact on medical image scan [28]. Herbulot and et al. [29] utilized the gradient of geometric shapes to segment the particular image targets. Additionally, in 2007, Li [30] applied the active contours for the energy stabilization of binary images. In 2009, Ni [31] used a local histogram and the active contour technique to segment-specific regions of the investigated images. Le and et al. [32] suggested a controlled active contour for adjusting energy function parameters.

Studies in machine learning has recently focused on deep learning-based techniques for classifying and sizing purposes, which are one of the new and automated plans [33,34]. Studies have evolved several methods to combine DL techniques with Active Contour Models (ACM). Several attempts have been made to incorporate an efficient Loss Function (LF) based on the ACM's energy function, including AC loss [35], active contour loss [36], Mumford-Shah loss [37], and level-set loss [38]. Meanwhile, some researchers attempted an end-to-end (e2e) process that combined ACM and DL techniques. The level-set strategy was used by Hu et al. [39] to help networks recognize salient items more precisely; however, its success is highly dependent on the unusual tweaking of parameters and the level-set structure. DARNet [35] and DSAC [40], for example, trained a convolutional neural network (CNN) to learn ACM parameterizations.

Although these structures lack efficiency and robustness, they are nevertheless susceptible to hand-operated target contour initialization. Hatamizadeh et al. [41] have developed a novel DALS structure that combines CNN and ACM to separate distinct lesions in medical imaging. To train ACM, DALS cannot be used because it is typically used as a post-processing step. To segment medical images, a Deep Active Contour Network (DACN) was developed [16]. An all-inclusive differential training strategy enabled them to accurately identify object boundaries.

An interactive medical images segmentation based on active contours with enhanced F energy in level-set tuning is proposed in the current study to solve the shortcomings of prior methods. The segmentation approach is used with an AC-designed algorithm and upgraded Level-set procedures to produce parameter maps in the proposed model. The initial contours of ACM are optimized directly based on F energy. As a result, the proposed structure functions as a differentiable and self-contained framework. The BI-RADS dataset and mini-mias mammography pictures are used to evaluate our technique. Furthermore, as shown by the extra trimap analysis, the segmentation technique acquired by the suggested structure provides a more refined representation of object edges. The following are the major contributions of our research:

1- We apply pre-process step based on Highboost trick to refine the map of the active counters. As a result, the explored edges are clear to obtain the proper object border. Consequently, the *F* energy function in Level-set is tuned based on the cleared map.
2- The enhanced Level-set method and F function selection help fast stabling and detecting the border of objects in medical images.
3- Computational complexity has been avoided, and the speed of the method has been significantly increased. Therefore, the suggested method may take less time to find the target region of the medical image.

This article's remaining sections are laid out as follows: Section 2 discusses the suggested active contour approach, and Section 3 demonstrates the model's implementation and outcomes. Eventually, the conclusion is outlined in Section 4.

2. PROPOSED MODEL

2.1. Pre-Processing

In medical images, the shape and margin are two significant criteria for diagnosing abnormal tissues from normal tissues. In particular, these images contain crucial information from the masses, primarily when the mass is concentrated in cancer cells. In this step, the images are sharpened by using the high-boost filter. In most cases, due to different reasons, the medical images are lacking in defining the details. Whereas in spatial domains, blurring is done by calculating the mean of pixels in the neighborhood region; thus, these mean

calculations areas are the same as integration; therefore, it can be concluded that sharpening by the derivative operator is possible. The response strength of the derivative operator is proportional to discontinuous intensity. Thus, derivation from an image enhances the edges and other discontinuous segments and blurs the pixels with low-intensity variation. Sharpener filters based on derivatives, specifically first and second order, is sharpened the image by multiplying the derivate image with the original image. In this paper, we used a Laplacian filter to sharpen the details of the image. To express the Laplacian equation as discrete form, equation (1) can be described as:

$$\nabla^2 f = [f(x+1,y)+f(x-1,y) \\ +f(x,y-1)+f(x,y-1)]-4f(x,y) \quad (1)$$

F(x,y) is the reference image, and ∇ shows the implementation of the two-dimensional Laplacian operator. Hence, the operator is applied to two images, and an anisotropic result for rotations in increments of 90 degrees is achieved. According to described filters, the entire was deducted from the different terms. In Fig. 1, two matrixes that can boost the image are shown.

$$\begin{bmatrix} 0 & 1 & 0 \\ 1 & -4 & 1 \\ 0 & 1 & 0 \end{bmatrix} \begin{bmatrix} 1 & 1 & 1 \\ 1 & -8 & 1 \\ 1 & 1 & 1 \end{bmatrix}$$

Fig. 1. The Laplacian filter is applied images based on two main mapping matrixes as highboost filter.

The outcome of applying the Laplacian filter to the image containing the high-boost filter is depicted in Fig. 2. In Fig. 2, some information is boosted to help border detection through ACMs. The displayed images in *a* and *c* are the reference images that are sharpened by a high boost filter. Images *b* and *d* show the result of the Laplacian filter. The clarity of the border is achieved by using the high boost filter.

2.2. Active contour model

Image forces and external energies are used to control and guide ACM in image space, which may be described as a parametric spline:

$$S(u) = I(x(u), y(u)) \quad (2)$$

Where, u is [0,1] and is transformed by an energy function that leads to interesting features such as boundaries, edges, and lines. Energy function can be defined as [42]:

$$E = \int_0^1 E_{snake} S(u) du \quad (3)$$

Where contains internal and external energies. The ACM drives into alignment with the local energy minimum of an image features of an edge. An image's energy function is reduced by shifting the curve around its spatial field, which may be expressed mathematically as:

$$E = \int_0^1 [E_{\text{int}}.S(u) + E_{img}.S(u)] du \quad (4)$$

The first phase E_{int} describes the internal energy responsible for the smoothness and deformation method of the contour. In simple words, internal energy depends on features of contour such as elastic curve, which is generated from the image and can be represented as (5):

$$E_{\text{int}} = (0.5 \times a \times \int \left| \frac{\partial}{\partial u} S(u) \right|^2 du) \\ +(0.5 \times b \times \int \left| \frac{\partial^2}{\partial u^2} S(u) \right|^2 du) \quad (5)$$

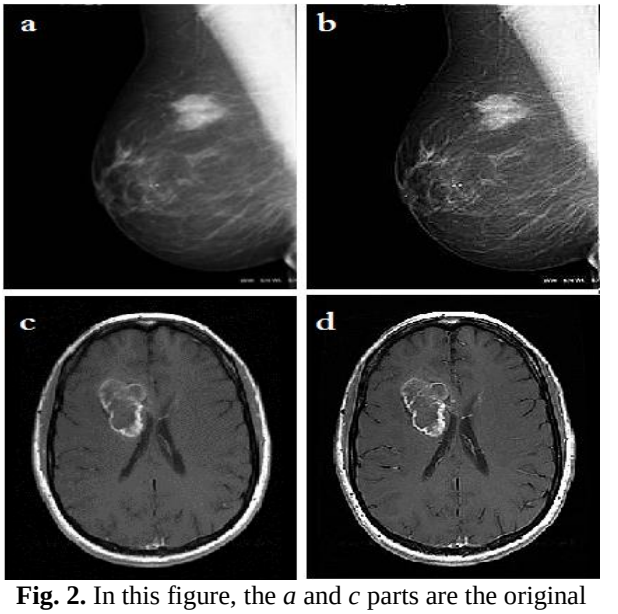

Fig. 2. In this figure, the *a* and *c* parts are the original images, and *b* and *d* are sharpened images by the highboost filter.

Where, *a* and *b* are weighted parameters of elasticity and rigidity, respectively. These parameters control the sensitivity of contour. The first term of internal energy causes the contour to behave like a spring and determines the elastic ratio of the curve. Besides, the rigidity ratio of the curve is specified by the second part of internal energy. A technique known as "image energy" allows the active contour to be steered to the most visible visual features such as lines, corners, and edges. In the early equation of the active contour, it's called "edge detection," so this is how it is defined:

$$E_{img} = E_{edge} = -\rho \left| \nabla I(s) \right|^2 \quad (6)$$

or:

$$E_{img} = E_{edge} = -\rho\left|\nabla(G(s) * I(s))\right|^2 \quad (7)$$

This equation is used to reduce the noise, and *p* is the parameter that presents the magnitude of image energy, gradient operator, *G(s)* image convolution with Gaussian filter, and variance. Consequently, the total energy of active contour can be described as:

$$E_{\text{int}} = (0.5 \times a \times \int \left|\frac{\partial}{\partial u} S(u)\right|^2 du) + \int E_{edge}.S(u)du + (0.5 \times b \times \int \left|\frac{\partial^2}{\partial u^2} S(u)\right|^2 du) \quad (8)$$

In the presence of dominant image features, the energy function leads the contour towards a valid form. Still, unfortunately, in the lack of sharp edges, the contour curve has a problem detecting the target segment. New energy is defined as color energy replaced to edge energy in equation (8) to overcome this difficulty. As a result of statistics, this pressure energy is released as an explosion or a contraction of the contour toward the desired location. Color pressure energy can be denoted as:

$$E_{pre} = rG(I(s))(\frac{\partial}{\partial u})^{\perp} \quad (9)$$

Where *r* is a parameter to assign the magnitude of pressure energy and initialize by the operator. Parameter *G* is a model that can be expressed as:

$$G(I(s)) = \begin{cases} +1 & I(s) \geq T \\ -1 & otherwise \end{cases} \quad (10)$$

Where, *T* is the intensity threshold, and another definition of the *G* function is:

$$G(I(s)) = \begin{cases} +1 & (I(s) - m) \times s^{-1} \leq k \\ -1 & otherwise \end{cases} \quad (11)$$

K is a constant, *M* is average, and *S* is the variance of target pixels values that exist as rudimentary data or achieved from the image. To segment and minimize the energy criterion, the model of the active contour can be introduced as (12):

$$\frac{\partial \phi}{\partial t} = \delta_0(\phi).\Re \quad (12)$$

where:

$$\Re = \mu div(\frac{\nabla \phi}{|\nabla \phi|}) - v - \lambda_1(g - c_1)^2 + \lambda_2(g - c_2)^2 \quad (13)$$

g is the gray-level image, $\delta_0(\varphi)$ is the Dirac evaluation function (i. e., derivative of Heaviside function), c_2 and c_1 are the averages of *g* at outside and inside the propagated curve. The μ, ν and λ_1, λ_2 are stabilizer parameters and must be μ ≥ 0 and ν ≥ 0 λ_1, λ_2 > 0.

2.3. Optimized Level-set

The proposed algorithm, which is varied in some parameters, is the Level-set method. If $\varphi(x,y,t)$ space of image assumes as a level curve (contour) for every (x,y) point, then $\varphi(x,y)$ has obtained a value proportionate to the function of $\varphi(x,y,t)$. By assuming $C(t)$ as propagated curve and the zero level-set of the procedure for all *t*, then:

$$\phi(C(t),t) = 0 \quad (14)$$

By derivation from equation (14) respecting *t* and by using the chain rule, equation (15) can be defined as:

$$\phi_t + \nabla\phi.C_t = 0 \quad (15)$$

This equation is derived from heat equations and contains two parts, partial derivatives, and spatial derivatives. If extension speed of contour in different dimensions is defined as *F*, then equation (16) can be obtained as:

$$F = C_t.n \quad (16)$$

where $n = (\nabla\varphi)/(|\nabla\varphi|)$ and so the equation (15) can be remarked as equation (17):

$$\phi_t + F|\nabla\phi| = 0 \quad (17)$$

It can be inferred that this equation is yielded from the finite difference approximation for spatial and time derivatives considering $\varphi(c,t=0)$. In the AC model, several types of energy are affected by the convergence of the system. By selecting a proper *F* function, it can have efficacy on convergence and accuracy of the system. We proposed equation (18) which has high speed and accuracy on convergence and target detection. The equation is a gradient detection function.

$$g(x,y) = (1 + |I(x,y) * \nabla G_\sigma|)^{-1} \quad (18)$$

The gradient of an image is used to extract information and data from an image. Indeed, the gradient is the evaluation of instantaneous variation in the intensity criterion of pixels. The gradient is a vector, and in the image, it is in horizontal or vertical dimensions. In the image, one of the particular applications of the gradient is edge identification. By the composition of equation (15) and gradient detection equation, the conclusive function of level-set is achieved as equation (19):

$$\phi_t = g(x,y)|\nabla\phi|(F_0 + div(\frac{\nabla\phi}{|\nabla\phi|}) \quad (19)$$

All steps of the contour model and level-sets have been shown in Table 1.

Table 1: steps of the proposed algorithm of ACM and the Level-set.

The steps of the proposed algorithm of ACM and the Level-set
1. *Start*
Initialize □ function for determination of initial curve
2. The Spatial derivatives creation
2.1 *Using finite differences in the spatial derivatives.*
2.2 *Initial calculation of* $\square_T$.
3. Assigning *F* (speed of contour) in separation with proposed F function
4. locality increase and movement of □ by using new value of □ and $\square_T$ and update them
5. Repeat step 2 to 4.
6. Stop algorithm
7. *end*

3. EXPRIMENTAL RESULTS

The suggested model is examined on a database of medical images. For the research case, we have used 80 mammography images (40 healthy and 40 cancerous breast women) [43], 80 brain tumor MR images (i. e., 30 healthy and 50 subjects with tumors).

The related mammography images are received from South Florida (USA), a database that is the cancerous breast or suspicious regions detected by physician radiologists and BI-RADS [44]. The used Brain images are also from the WEB database, which is noisy less than 5%. The MR images were from batch T1-Weighted images. Among 70 healthy tissue images, the system is just detected seven images wrong. In another case, the system is used for 90 illness and virulent tumor images, making four errors. In the rest of the images, the system diagnosed the cancerous tissues successfully.

Accuracy (Acc), recall (Re), precision (Pr), Hausdorff distance (HaD), and dice (Di) are criteria that are used to measure efficiency. In addition, we perform a trimap analysis [45,46]. In the trimap test, assessment metrics are calculated solely in the object border area, not the entire image. The evaluation domain is formed by tracing a W pixel band around the edges of objects, with *W* being the target area's width. For users concerned in contours, trimap analysis is a more relevant determination. Additionally, we evaluate Dice's ability to characterize lines and borders in such edge-adjacent regions of varying widths. These evaluation parameters are calculated as the average value for both datasets. Table 2 shows the evaluation factors. Finally, the conclusive average value of these parameters is computed for both databases which the accuracy, recall, and precision are 96.25%, 95.60%, and 95.71%, respectively.

4. DISCUSSION

As Table 3 shows, the system has a satisfactory ability to segment tumors based on the ACM with optimized *F* function, pre-processing, and designed initializing compared to two popular ACM in segmentation procedure. Images from the WEB database as well as those from the Table 3 mini-mias dataset were used in these two methods. On both datasets at once, the suggested system was evaluated to assess how well it performed. Whereas the system is a binary state in performance, and thus, the proposed approach is assayed by the operational criterion of the ROC curve compared to both the Le et al. [32] and Yang et al. [47] methods in mammography images. The maximum specificity and sensitivity are obtained when the operation point adapts to the optimized point. Fig. 3 shows the ROC plot for three methods and 40 random images from 160 shown images.

Table 2. The average quantitative examination of various states for the proposed method on two datasets.

Method	P	Re	Acc	Di	HaD
ACM with normal Level-Set	0.9008	0.9116	0.9272	0.9008	44.98
ACM with optimized *F* function	0.9109	0.9264	0.9329	0.9017	36.12
ACM with optimized *F* function and pre-processing	0.9389	0.9412	0.9411	0.9328	28.74
ACM with optimized *F* function, pre-processing and designed initializing	0.9571	0.9560	0.9625	0.9474	22.18

Table 3. Valid segmentation approaches for mammography and the brain compared to the suggested system images.

Method	P	Re	Acc	Di	HaD
DACN [16]	0.9076	0.8432	0.9319	0.8463	24.46
Le [32]	0. 8976	0. 8866	0.9011	0.8355	38.67
Yang [47]	0. 9311	0. 9472	0.9355	0.9145	23.89
Our model	**0.9571**	**0.9560**	**0.9625**	**0.9474**	**22.18**

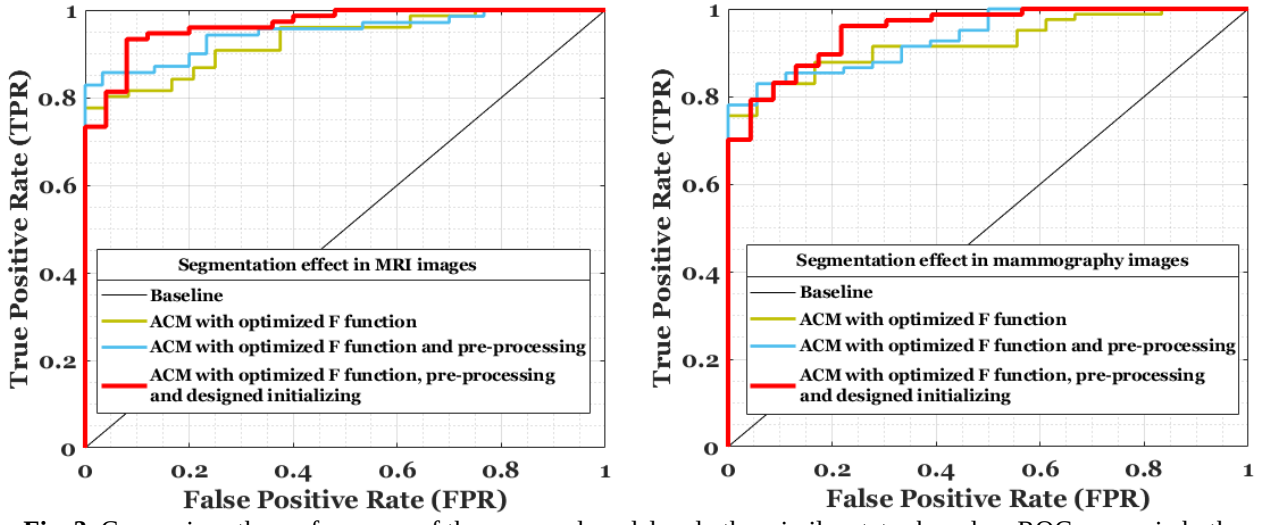

Fig. 3. Comparison the performance of the proposed model and other similar states based on ROC curves in both datasets.

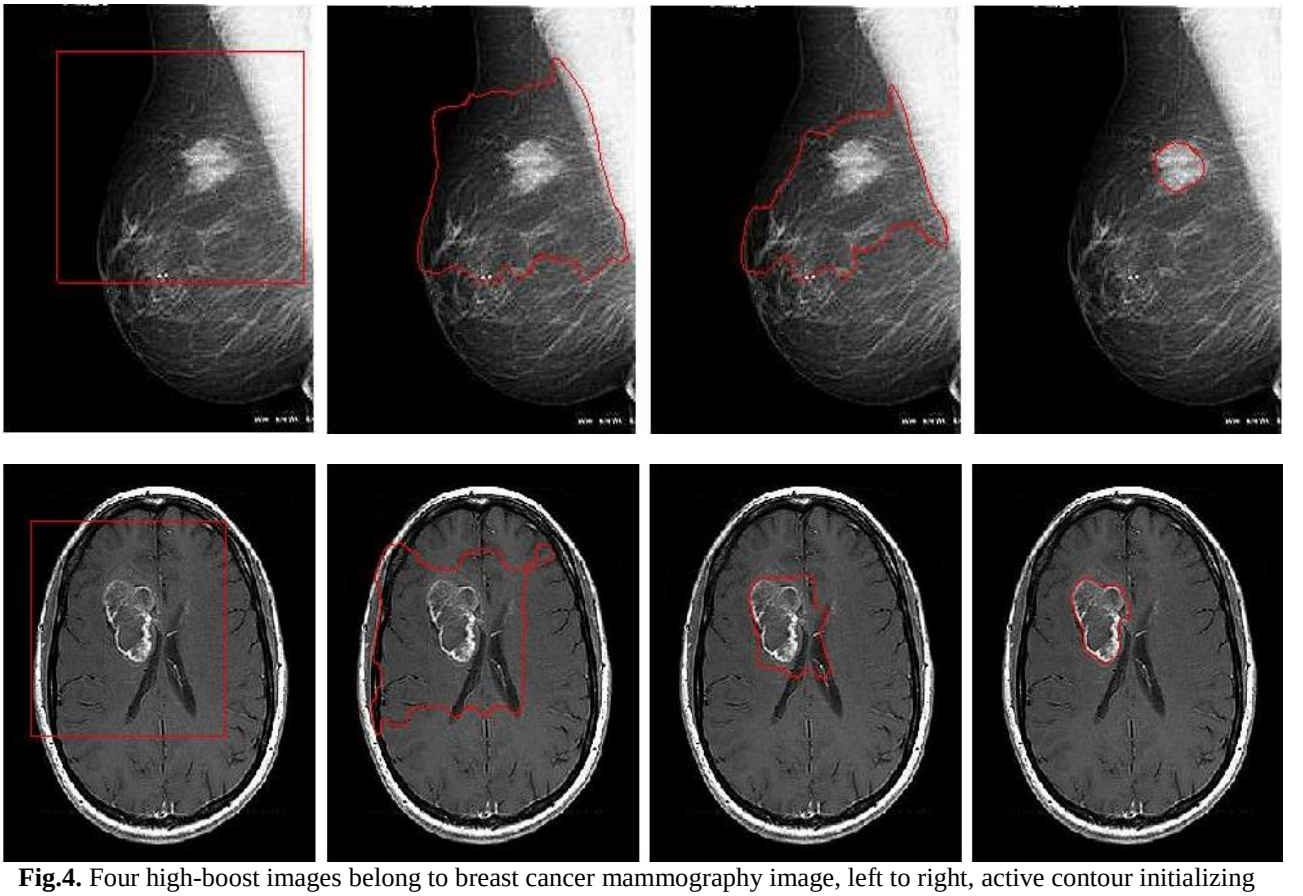

Fig.4. Four high-boost images belong to breast cancer mammography image, left to right, active contour initializing step on the original image, curve progress in 150 loop repeats, curve progress in 250 loop repeats, curve progress in 400 loop repeats. Four high-boost images belong to brain tumor MR image left to right, active contour initializing step on the original image, curve progress in 150 loop repeats, curve progress in 250 loop repeats, curve progress in 400 loop repeats.

The overlap percentage of the proposed method, whatever physicians and radiologists were expressed, is

about 75.00%, while such criteria for the Yang et al [47] and Zhang are 70.00% and 65.00%, respectively. These statistic differences are meaningful considerably for physician experts (p Value < 0.01). Fig. 4 shows all implementation steps which obtained high accuracy detection for cancer tumor for two images.

Fig. 5 show the level-set output as 3D plots for mammography and MR image. The significant preference of the proposed algorithm against other same methods in literature is rapid convergence and high accuracy. In most literature, the number of pixels is an essential parameter to convergence. If this parameter exceeds, the algorithm faces errors. Still, in the proposed algorithm, medical images with high content can also process, and tumors can segment with a few repeat loops.

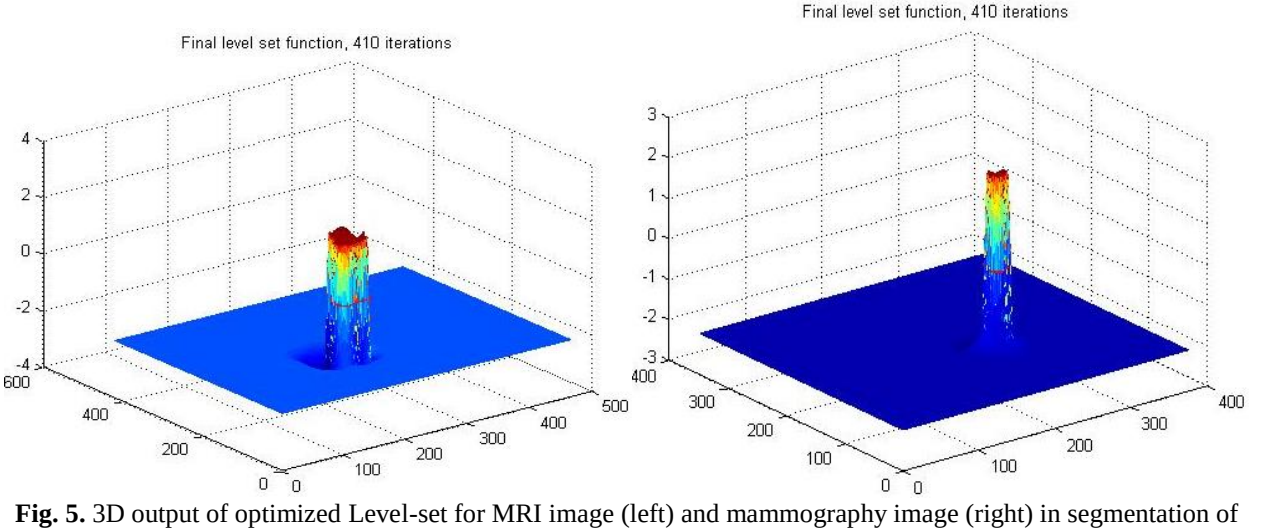

Fig. 5. 3D output of optimized Level-set for MRI image (left) and mammography image (right) in segmentation of tumours.

Tables 2 and 3 show the quantitative comparison of different approaches on two MR and mammography images. The proposed ACM model performs better than all other models, including the optimized AC or Level-set structure and existing state-of-the-art approaches. Table 3 shows the empirical outcomes on both datasets. Our model performs best in Hausdor Distance (22.18), Recall (0.9560), and Dice (0.9474). Compared to the baseline CNN architectures (i. e., similar DACN [16]) with a significant improvement (3.5%), they suggest that the proposed model performs fewer false negatives (FN). Our model's accuracy (0.9625) is close to that of the best (0.95). Although the proposed structure's precision is lower than CNN architectures, it is still relatively high.

It is also worth noting that our ACM with optimized Level-set delivers consistent Hausdor Distance results on both image sets. The HaD calculates the span between two surfaces, demonstrating that the suggested ACM results in more exact object boundary localization.

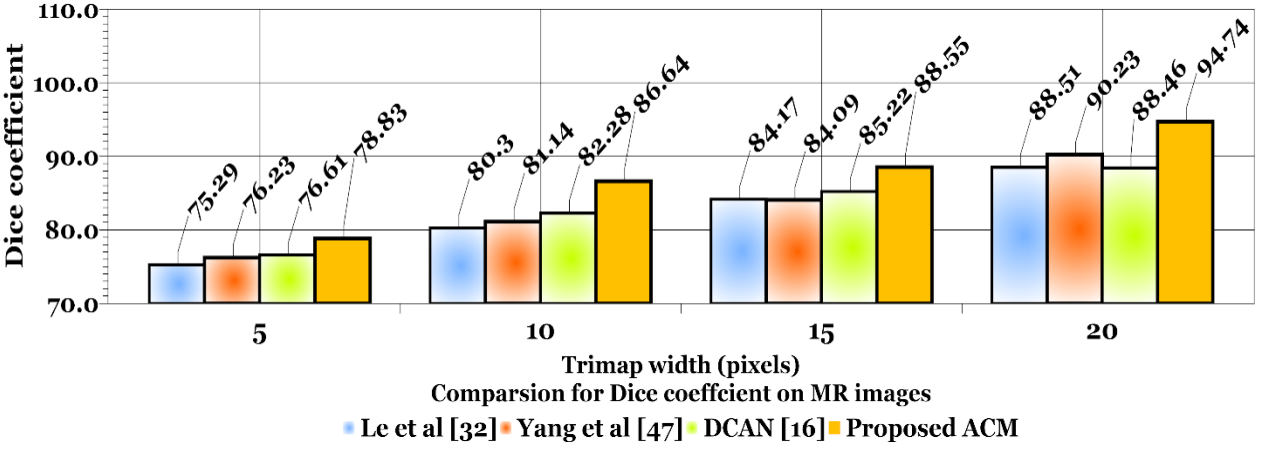

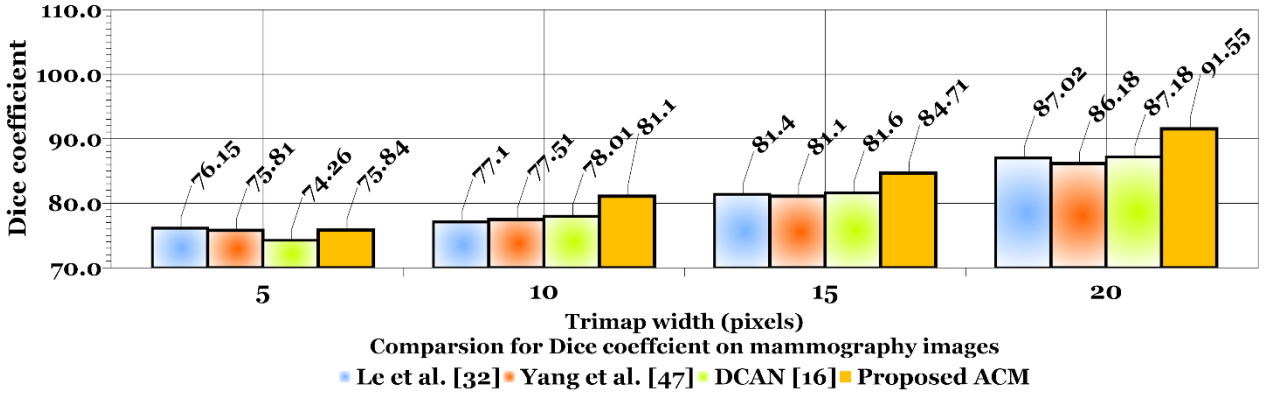

Fig. 6. The effects of the trimap analysis on two image sets. The illustrated bar chart about trimap analysis on MR images (Top chart). The same bar chart on mammography images (Bottom chart). Dice is measured in the area circling the tumor borders, where trimap width depicts the band of this area.

Segmentation outcomes of various approaches are revealed in Fig. 6. The target lines of borders are difficult and low-contrast to the background of original image, therefore losing CNN architectures. Nevertheless, in such states, the proposed ACM still produces nearly accurate prediction maps. Trimap analysis is used to measure the depiction of edges and borders. In Fig. 6, we show bar charts concerning linked outcomes to examine various models' quality. On both datasets, our model achieves higher Dice in all settings than CNN structures (such as DACN [16] and related models). The mentioned outcomes show that the proposed model has an influential ability to recognize accurate tumors or object borders, profiting from the utilization of ACMs.

5. CONCLUSION

The purpose of this article is to describe a technique for detecting the borders of malignant masses. This system performs well in terms of speed and accuracy, and it is more powerful when it comes to combining related tasks. High processes in low time for high dimensions images are advantages that make a special performance from other similar methods. The proposed algorithm can extract tumors from medical images at a prominent level. One hundred sixty mammograms and MR images were taken from two medical images datasets with optimum accuracy, recall, and precision equal to 96.25%, 95.60%, and 95.71%. In the future, we implemented this algorithm on multiple images from various datasets. In addition, our proposed ACM model with preprocessing step, optimized Level-set, and automatic initializing can further be utilized to Multiclass Semantic Segmentation (MSS), where the problem of MSS should be decomposed into different single class segmentations. Additional research on the workings of our ACM's mechanism will be carried out in the future. We will see whether we can incorporate CNN structures into the proposed model.

6. ACKNOWLEDGMENT

We owe a debt of gratitude to Meybod University and the Islamic Azad University of Torbat-e Jam for their unwavering assistance. The authors would like to thank the physicians and radiologists at Sabzevar's Vasei Hospital's Medical Image Center for their help in completing this study.

REFERENCES

[1] A. Rezaee, K. Rezaee, J. Haddadnia and H. T. Gorji, "**Supervised metaheuristic extreme learning machine for multiple sclerosis detection based on multiple feature descriptors in mr images**", *SN Applied Sciences*, Vol. 2, pp. 1-19, 2020.

[2] F. Ozdemir, Z. Peng, P. Fuernstahl, C. Tanner, O. Goksel, "**Active learning for segmentation based on Bayesian sample queries**", *Knowledge-Based Systems*, Vol. 214, 106531, 2021.

[3] K. Rezaee, A. Badiei, S. Meshgini, "**A hybrid deep transfer learning based approach for COVID-19 classification in chest X-ray images**", *In 2020 27th National and 5th International Iranian Conference on Biomedical Engineering (ICBME)*, pp. 234-241, 2020.

[4] K. Rezaee, A. Rezaee, N. Shaikhi, J. Haddadnia, "**Multi-mass breast cancer classification based on hybrid descriptors and memetic meta-heuristic learning**", *SN Applied Sciences*, Vol. 2, no. 7, pp. 1-19, 2020.

[5] T. Kim, and et al., "**Active learning for accuracy enhancement of semantic segmentation with CNN-corrected label curations: Evaluation on kidney segmentation in abdominal CT**", *Scientific reports*, Vol. 10, no. 1, pp. 1-7, 2020.

[6] K. Rezaee, and et al, "**Multi-mass breast cancer classification based on hybrid descriptors and memetic meta-heuristic learning**", SN Applied Sciences 2, No. 7, pp. 1-19, 2020

[7] K. Rezaee and J. Haddadnia, "**Designing an Algorithm for Cancerous Tissue Segmentation Using Adaptive K-means Cluttering and Discrete Wavelet Transform**", *J Biomed Phys Eng*., Vol. 3, No. 3, pp. 93-104, Sep 2013.

[8] Y. Shi, M. Li, W. Zeng, "**MARGM: A multi-subjects adaptive region growing method for group fMRI data analysis**", Biomedical Signal Processing and Control, Vol. 69, pp. 102882, 2021.

[9] T. Wu, Z. Yang, "**Animal tumor medical image analysis based on image processing techniques and embedded system**", Microprocessors and Microsystems, vVol. 81, 103671, 2021.

[10] Y. Alzahrani, Y., B. Boufama, "**Biomedical Image Segmentation: A Survey**", SN Computer Science, vol. 2, no. 4, pp. 1-22, 2021.

[11] F. H. Araújo, R. R. Silva, F. N. Medeiros, J. F. R. Neto, P. H. C. Oliveira, A. G. C. Bianchi, D. Ushizima, "**Active contours for overlapping cervical cell segmentation**" International Journal of Biomedical Engineering and Technology 35, No. 1, pp. 70-92, 2021.

[12] K. Bi, Y. Tan, K. Cheng, Q. Chen, Y. Wang, Y, "**Sequential shape similarity for active contour based left ventricle segmentation in cardiac cine MR image**", Mathematical Biosciences and Engineering, Vol. 19, No. 2, pp. 1591-1608, 2022.

[13] G. Liu, G., and et al., "**Superpixel-based active contour model via a local similarity factor and saliency**", Measurement, No. 110442, 2021

[14] R. Zhang, M. You, "**Fast contour detection with supervised attention learning**", Journal of Real-Time Image Processing, Vol. 18, No. 3, pp. 647-657, 2021.

[15] Y. Lei, and G. Weng, "**A robust hybrid active contour model based on pre-fitting bias field correction for fast image segmentation**", Signal Processing: Image Communication, No. 116351, 2021.

[16] B. D. M. Zhang and Q. Li, "**Deep active contour network for medical image segmentation**", *Medical Image Computing and Computer-Assisted Intervention* - MICCAI 2015, 2020.

[17] Y. Yang, R. Wang, H. Ren, "**Active contour model based on local intensity fitting and atlas correcting information for medical image segmentation**" *Multimedia Tools and Applications*, pp. 1-17, 2021.

[18] S. Husham, A. Mustapha, S. A. Mostafa, M. K. Al-Obaidi, M. A. Mohammed, A. I. Abdulmaged, et al., "**Comparative analysis between active contour and otsu thresholding segmentation algorithms in segmenting brain tumor magnetic resonance imaging**", *J. Inf. Technol. Manage*., vVol. 12, pp. 48-61, Dec. 2020.

[19] M. Sharif, U. Tanvir, E. U. Munir, M. A. Khan and M. Yasmin, "**Brain tumor segmentation and classification by improved binomial thresholding and multi-features selection**", *Journal of Ambient Intelligence and Humanized Computing*, pp. 1-20, 2018.

[20] J.A. Sethian, **"Evolution, Implementation, and Application of Level Set and Fast Marching Method**s **for Advancing Fronts**", *Journal of Computational Physics* Vol. 169, pp. 503–555, 2001.

[21] D. Adalsteinsson, J.A. Sethian, "**A Fast Level Set Method for Propagating Interfaces**", *J.Comp.Phys.* pp.269~277, 1995.

[22] S. Osher, R. Fedkiw, "**Level Set Methods and Dynamic Implicit Surface**", *Springer¬Verlag*, 2002.

[23] D Terzopoulos, D Metaxas. "**Dynamic 3D Models with Local and Global Deformations: Deformable Superquadrics**." *IEEE Transactions on Pattern Analysis and Machine Intelligence* Vol. 13, no. 7, pp.703-715, 1999.

[24] J. Weickert and G. Kuhne, "**Fast methods for implicit active contour models**", *in Geometric Level Set Methods in Imaging Vision and Graphics*, New York:Springer-Verlag, 2003.

[25] M. Holtzman-Gazit, D. Goldshe, and R Kimmel. "**Hierarchical segmentation of thin structure in volumetric medical images**". *In: Medical image computing and computer-assisted intervention (MICCAI)*, Montreal; 2003.

[26] C. Rother, V. Kolmogorov, and A. Blake, "**GrabCut: interactive foreground extraction using iterated graph cuts**", *ACM Transactions on Graphics (TOG)*, Vol.23, No.3, August 2004.

[27] C. Pluempitiwiriyawej, JMF. Moura, Yi-Jen Lin Wu and Chien Ho. "**STACS: New Active Contour Scheme for Cardiac MR Image Segmentation**", *IEEE Transactions on Medical Imaging*, Vol. 24, No. 5, pp 593-602, May 2005.

[28] Y. Boykov and G. Funka-Lea, "**Graph Cuts and Efficient N-D Image Segmentation**". *In International Journal of Computer Vision (IJCV)*, Vol. 70, No. 2, pp. 109-131, 2006.

[29] Herbulot, S. Jehan-Besson, S. Duffner, M. Barlaud, and G. Aubert. "**Segmentation of vectorial image features using shape gradients and information measures**". *Journal of Mathematical Imaging and Vision*, 25(3):365–386, October 2006.

[30] C.M. Li, C. Kao, J. Gore, Z. Ding, "**Implicit active contours driven by local binary fitting energy**", *IEEE Conference on Computer Vision and Pattern Recognition*, 2007.

[31] K. Ni, X. Bresson, T. Chan, and S. Esedoglu. "**Local histogram based segmentation using the wasserstein distance**". *International Journal of Computer Vision*, Vol. 84, pp. 97–111, August 2009.

[32] N. Le, T. Bui, V. K. Vo-Ho, K. Yamazaki, K. Luu, "**Narrow Band Active Contour Attention Model for Medical Segmentation**", *Diagnostics*, Vol. 11, no. 8, pp. 1393, 2021.

[33] K. Rezaee, S. M. Rezakhani, M. R. Khosravi, M. K. Moghimi, "**A survey on deep learning-based real-time crowd anomaly detection for secure distributed video surveillance**", *Personal and Ubiquitous Computing*, pp. 1-17, 2021.

[34] K. Rezaee, S. Savarkar, X. Yu, J Zhang, "**A hybrid deep transfer learning-based approach for Parkinson's disease classification in surface electromyography signals**", *Biomedical Signal Processing and Control*, vol. 71, pp. 103161, 2022.

[35] X. Chen, B. M. Williams, S. R. Vallabhaneni, G. Czanner, R. Williams and Y. Zheng, "**Learning active contour models for medical image segmentation**", *Proc. IEEE/CVF Conf. Comput. Vis. Pattern Recognit. (CVPR)*, pp. 11632-11640, Jun. 2019.

[36] S. Gur, L. Wolf, L. Golgher and P. Blinder, "**Unsupervised microvascular image segmentation using an active contours mimicking neural network**", *Proc. IEEE Int. Conf. Comput. Vision*, pp. 10 722-10 731, 2019.

[37] B. Kim and J. C. Ye, "**Mumford–shah loss functional for image segmentation with deep learning**", *IEEE Trans. Image Process*., Vol. 29, pp. 1856-1866, 2020.

[38] Y. Kim, S. Kim, T. Kim and C. Kim, "**CNN-based semantic segmentation using level set loss**", *Proc. IEEE Winter Conf. Appl. Comput. Vis.* (WACV), pp. 1752-1760, Jan. 2019.

[39] P. Hu, B. Shuai, J. Liu and G. Wang, "**Deep level sets for salient object detection**", *Proc. IEEE Conf. Comput. Vis. Pattern Recognit*., pp. 540-549, 2017.

[40] D. Marcos, D. Tuia, B. Kellenberger, L. Zhang, M. Bai, R. Liao, et al., "**Learning deep structured active contours end-to-end**", *Proceedings of the IEEE Conference on Computer Vision and Pattern Recognition*, pp. 8877-8885, 2018.

[41] A. Hatamizadeh, A. Hoogi, D. Sengupta, W. Lu, B. Wilcox, D. Rubin, et al., "**Deep active lesion segmentation**", *International Workshop on Machine Learning in Medical Imaging (MLMI).*, pp. 98-105, 2019.

[42] E. E. Nithila and S. S. Kumar, "**Segmentation of lung from CT using various active contour models**", *Biomed. Signal Process. Control*, Vol. 47, pp. 57-62, 2019.

[43] J. Suckling, J. Parker, D. R. Dance, S. Astley, I. Hutt, C. R. M. Boggis, et al., "**The mammographic image analysis society digital mammogram database**", *in Proc. 2nd Int. Workshop Digit. Mammography*, U.K., York, pp. 375-378, Jul. 1994.

[44] https://www.med.harvard.edu/aanlib/home.html.

[45] L.-C. Chen, Y. Zhu, G. Papandreou, F. Schroff and H. Adam, "**Encoder-decoder with atrous separable convolution for semantic image segmentation**", *Proc. ECCV*, pp. 801-818, Sep. 2018.

[46] P. Kohli, P. H. Torr and L. Ladick, "**Robust higher order potentials for enforcing label consistency**", *Int. J. Comput. Vis.*, Vol. 82, No. 3, pp. 302-324, 2009.

[47] Y. Yang, X. Hou, H. Ren, "**Efficient active contour model for medical image segmentation and correction based on edge and region information**". *Expert Systems with Applications*, pp. 116436, 2022.